Hybrid Graphene-Plasmonic Gratings to Achieve Enhanced Nonlinear Effects at Terahertz Frequencies

Tianjing Guo, Boyuan Jin, and Christos Argyropoulos[*]

Department of Electrical and Computer Engineering, University of Nebraska-Lincoln, Lincoln, Nebraska 68588, USA

High input intensities are usually required to efficiently produce nonlinear optical effects in ultrathin structures due to their extremely weak nature. This problem is particularly critical at low terahertz frequencies because high-input-power terahertz sources are not available. The demonstration of enhanced nonlinear effects at terahertz frequencies is particularly important since these nonlinear mechanisms promise to play a significant role in the development and design of new reconfigurable planar terahertz nonlinear devices. In this work, we present an alternative class of ultrathin nonlinear hybrid planar terahertz devices based on graphene-covered plasmonic gratings exhibiting very large nonlinear response. The robust localization and enhancement of the electric field along the graphene monolayer, combined with the large nonlinear conductivity of graphene, can lead to boosted third-harmonic-generation and four-wave-mixing nonlinear processes at terahertz frequencies. These interesting nonlinear effects exhibit very high nonlinear conversion efficiencies and are triggered by realistic input intensities with relatively low values. In addition, the third-harmonic-generation and four-wave-mixing processes can be significantly tuned by the dimensions of the proposed hybrid structures, the doping level of graphene, or the input intensity, whereas the nonlinear radiated power remains relatively insensitive to the incident angle of the excitation source. The nonlinear hybrid graphene-covered plasmonic gratings presented have a relative simple geometry and, as a result, can be used to realize efficient third-order nonlinear terahertz effects with a limited fabrication complexity. Several new nonlinear terahertz devices are envisioned on the basis of the proposed hybrid nonlinear structures, such as frequency generators, all-optical signal processors, and wave mixers. These devices are expected to be useful for nonlinear terahertz spectroscopy, noninvasive terahertz subwavelength imaging, and terahertz communication applications.

I. INTRODUCTION

Graphene is a two-dimensional (2D) material with unique electric and optical properties [1,2]. Surface plasmons are formed at its surface when it is excited by terahertz radiation [3], a property of paramount interest for a material to be used in the envisioned integrated terahertz plasmonic systems [4]. In addition, the conductivity of graphene can be dynamically controlled and tuned by electrostatic doping, usually by use of a gate-voltage configuration [5]. The tunable and reconfigurable functionalities of graphene have recently been widely investigated with the goal to design different adaptive graphene-based terahertz devices, such as polarizers [6], cloaks [7], phase shifters [8], optical modulators [9], and absorbers [10]. However, light absorption along a graphene monolayer is usually very weak due to its single-atom thickness, which is a deleterious property toward the practical applications of graphene-based devices [11].

Fortunately, the absorption can be enhanced by the patterning of doped graphene monolayers into periodic nanodisks [12], combining graphene with insulating layers [13], or integrating graphene with microcavities [14]. Nevertheless, complicated fabrication procedures are required to fabricate most of the aforementioned graphene-based configurations, making these designs prone to fabrication imperfections and other limitations. Recently, the magnetic resonance of a metallic grating was used to enhance the absorption of graphene monolayers at terahertz frequencies [15]. This structure is easier to fabricate and can potentially be more practical for the design of compact terahertz devices. By the placement of a graphene monolayer over a metallic grating, strong and localized electric fields are obtained along the graphene when the plasmon modes of both graphene and the grating coincide. This grating design is different from the recently proposed hybrid plasmonic waveguide modulator loaded with graphene [16].

Graphene has strong nonlinear electromagnetic properties [17,18]. The second-order nonlinear response of a

_____

[*]christos.argyropoulos@unl.edu

graphene monolayer usually vanishes within the dipole approximation [19], since graphene has centrosymmetric properties. However, graphene has been experimentally demonstrated to possess a remarkably strong third-order nonlinear susceptibility $\chi^{(3)}$ at terahertz frequencies [20]. The strong third-order nonlinear response originates from the intraband electron transitions [21], as well as the resonant nature of the light-graphene interactions. Both of these effects are dominant under terahertz-radiation illumination. Specifically, the Kerr nonlinear susceptibility $\chi^{(3)}$ of graphene was found to reach high values (1.4×10^{-15} m^2/V^2) in recent experiments [22].

Two of the most-common third-order nonlinear processes are third-harmonic generation (THG) and four-wave mixing (FWM). In the case of THG, an incident wave (ω) interacts with the system to produce a wave with 3 times the incident-wave frequency (3ω) [23]. The significant advantage of THG compared with other nonlinear processes is that it can be achieved with a single-wavelength source. This nonlinear process can be used to realize higher transverse resolution for nonlinear imaging and microscopy techniques [24] and improved sensing [25]. THG has also been reported to be produced by graphene and few-layer graphite films but with relative low efficiency despite the large nonlinear graphene susceptibility [26,27]. FWM is another interesting third-order nonlinear process that has found a plethora of applications in nonlinear imaging, wavelength conversion, optical switching, and phase-sensitive amplification [28–32]. Differently from THG, in FWM, two pump photons of frequency ω_1 and one probe photon of frequency ω_2 are absorbed and mixed in the nonlinear medium and a photon of frequency $\omega_{\text{FWM}} = 2\omega_1 - \omega_2$ is generated and emitted. The FWM efficiency strongly depends on the field enhancement at the input pump and probe frequencies and proper phase-matching conditions [33]. The field enhancement along graphene and other 2D materials is usually very weak due to the poor coupling of the incident electromagnetic radiation to these ultrathin media. However, the phase-matching condition can be relaxed in the case of 2D materials, since they are extremely thin and phase cannot be accumulated along their thickness, in contrast to conventional bulk nonlinear materials. The increase in the nonlinear efficiency of 2D materials remains elusive and is the subject of intense ongoing research [34,35].

Usually, very high input intensities are required to produce third-order nonlinear effects from ultrathin nonlinear materials due to their extremely weak nature, leading to very low nonlinear efficiency [36]. This detrimental effect is particularly acute at low terahertz frequencies, since high-input-power terahertz sources do not exist [37]. The use of different plasmonic configurations has been demonstrated to efficiently boost nonlinear optical effects mainly due to the enhanced local electric fields and relaxed phase-matching conditions at the nanoscale [38–52]. Plasmonic effects can lead to enhanced effective nonlinear susceptibilities on the basis of different configurations that are composed of materials with weak intrinsic nonlinear properties. Yet, the plasmonic boosting of nonlinear effects has been mainly achieved in the infrared and visible spectrum, and the enhancement of nonlinearities at terahertz frequencies remains limited.

In the current work, we study an alternative approach to boost nonlinear effects, specifically at terahertz frequencies, based on ultrathin hybrid plasmonic structures. In particular, we investigate the potential of graphene-covered metallic gratings to dramatically amplify the inherently weak nonlinear response of conventional metallic gratings and isolated 2D materials [34]. More specifically, we demonstrate that the addition of graphene in the proposed hybrid plasmonic structures is of paramount importance for the boosting of different nonlinear processes. This is mainly due to three reasons: (a) the large field enhancement and confinement arising from the strong interference between the surface plasmon excited due to the graphene monolayer and the localized plasmon confined in the metallic grating [53–57]; (b) the high nonlinear response of graphene [58], which is further boosted in the presence of the strong localized fields despite its one-atom thickness; (c) the perfect-phase-matching condition that is achieved along the subwavelength thickness of graphene. For these reasons, the efficiency of THG and FWM processes will be greatly enhanced with the proposed graphene-covered grating structures. Furthermore, the third-order nonlinear graphene conductivity is a function of the Fermi energy or doping level of graphene [59]. This effect is used to dynamically control the terahertz third-order nonlinear processes achieved by our tuning of the doping level via a gate-voltage configuration [3,6]. The voltages required for the aforementioned tuning are relatively low, as demonstrated later. This tunable mechanism allows the efficient generation of enhanced reconfigurable terahertz nonlinearities and provides the possibility to develop adaptive graphene-based nonlinear terahertz devices [60–64].

To investigate the enhancement of the nonlinear response of the proposed graphene-covered plasmonic grating, we use full-wave numerical simulations based on the finite-element method by using COMSOL MULTIPHYSICS. The finite-element-method equations are substantially modified to include the appropriate nonlinear polarizabilities and currents in Maxwell's equations so we can accurately simulate the nonlinear effects presented. The full-wave simulations presented are ideal to calculate the nonlinear radiated power by integrating the power outflow over a surface that surrounds the device under study. This is an ideal simulation scenario to accurately compare the theoretical results obtained with potential experimental results from nonlinear experiments. The proposed

hybrid structure can be easily experimentally verified with conventional fabrication techniques. For example, graphene and the metallic grating can be separately fabricated, by chemical vapor deposition on a copper foil and electron-beam lithography [65,66], respectively, and then combined to create the proposed hybrid structure. The plasmonic grating and graphene can support plasmons only when they are excited by transverse-magnetic (TM)-polarized waves [67] in the currently used terahertz frequency range. Hence, TM-polarized incident waves are considered as the excitation source of the proposed system throughout this work.

The paper is organized as follows: First, we theoretically analyze the linear response of the proposed hybrid graphene-metal system by using its equivalent-circuit model. The validity of the theoretical method is verified by our comparison of several analytical results with full-wave simulations in Sec. II, and the effects of the geometrical dimensions, graphene Fermi level, and different incident angles are investigated. In Secs. III and IV we present the enhancement of the THG and FWM nonlinear processes caused by the proposed hybrid nonlinear graphene-covered plasmonic grating. By comparing the nonlinear performance of the proposed hybrid gratings with that of conventional nonhybrid structures, such as a bare graphene monolayer or a plain metallic grating, we demonstrate that the efficiencies of both THG and FWM are increased by multiple orders of magnitude. Moreover, it is shown that the enhanced nonlinear responses presented can be tuned by variation of the geometry of the proposed hybrid grating or the graphene doping level. Finally, we demonstrate the relative insensitivity of the proposed system to the angle of incidence when oblique incident illumination is considered.

II. PERFECT ABSORPTION OF TERAHERTZ RADIATION

The geometry of the proposed hybrid graphene-covered metallic grating is illustrated in Fig. 1(a). The grating is periodic in the x direction with period p and is assumed to be extended to infinity in the y direction. It is made of gold, with terahertz optical constants calculated by use of the Drude model: $\varepsilon_{L,Au} = \varepsilon_\infty - f_p^2/f(f - i\gamma)$, where $f_p = 2069$ THz, $\gamma = 17.65$ THz, and $\varepsilon_\infty = 1.53$ are derived from fitting of the experimental values [68]. The height and trench width of the grating are d and b, respectively. The ground plane is thick enough to be considered opaque to the impinging terahertz radiation, leading to zero transmission. During our theoretical analysis, we initially assume the metallic grating to be made of a perfect electric conductor (PEC), which is a good approximation since the electromagnetic fields minimally penetrate metals at low terahertz frequencies [69]. The grating is covered by a graphene monolayer sheet with doping or Fermi level E_F. Intraband transitions dominate the graphene response in the low terahertz-frequency range, and the linear conductivity of graphene can be expressed by use of the Drude formalism: $\sigma_g = (e^2 E_F/\pi\hbar^2)[j/(j\tau^{-1} - \omega)]$ [70], where e is the electron charge, $\hbar$ is the reduced Planck constant, $\omega = 2\pi f$ is the angular frequency, j is the unit imaginary number, and τ is the relaxation time [71], which is assumed to be 10^{-13} s [72,73] throughout this work. The relaxation time can be affected by many factors, such as temperature, Fermi level (doping), external field, graphene-sample quality, and the substrate material used [74–77].

The proposed structure is illuminated by a TM-polarized wave (the magnetic field in the y direction) with an incident angle θ with respect to the z direction. The inset on
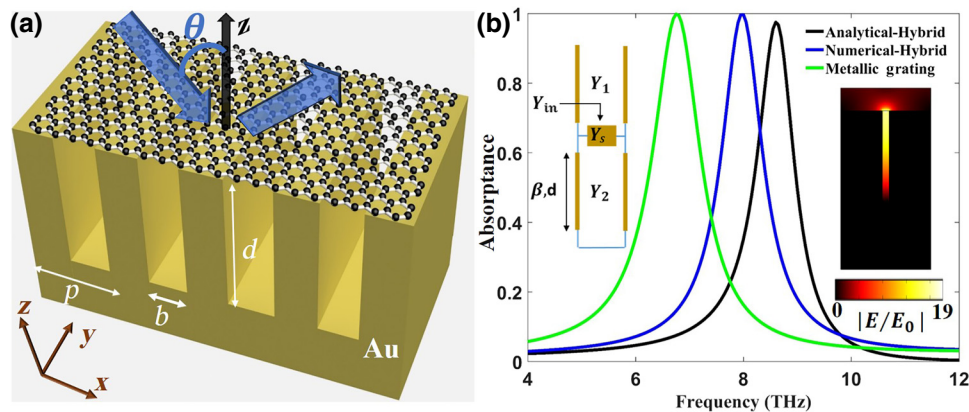

FIG. 1. (a) The hybrid graphene-covered gold grating. (b) Analytically (black line) and numerically (blue line) computed absorption spectra of the proposed hybrid grating. The absorption spectrum of the metallic grating without graphene on top is plotted as a green line. The results are obtained for grating parameters $p = 10$ μm, $b = 0.6$ μm, $d = 10$ μm. Graphene's Fermi level E_F is 0.3 eV. The left inset shows the equivalent-circuit model used to theoretically analyze the proposed structure. The right inset represents the computed electric-field-enhancement distribution at the resonant frequency of the hybrid grating.

the left in Fig. 1(b) shows the equivalent circuit [78] used to analytically model one unit cell of the graphene-covered grating, with $Y_1 = \omega \varepsilon_0 n/k_0$ and $Y_2 = \omega \varepsilon_0 n/k_0 (p/b)$ being the corresponding characteristic admittances of the surrounding air and grating trench regions, respectively. In these formulas, n is the refractive index of air around the grating and inside the grating trench and k_0 is the free-space wavenumber. The graphene sheet is modeled as an additional shunt admittance Y_s in the equivalent-circuit model that can be calculated by the simple formula $Y_s = \sigma_g (p/b)$. The reflection coefficient is computed by our applying transmission-line theory [79] to the proposed terahertz equivalent-circuit model and is given by $\Gamma = \{[Y_s - (j Y_2 \cot \beta d)]/[Y_1 + (Y_s - j Y_2 \cot \beta d)]\}$ [80], where β is the propagation constant in the grating-trench region. The absorptance can be computed by the relationship $A = 1 - |\Gamma|^2$ [12,15,81–83], since in the current grating configuration the transmission is zero. Alternatively, the total reflected power density from the hybrid grating can be used to compute the absorptance by use of the formula $A = 1 - (P_{\text{ref}}/P_{\text{in}})$, where P_{ref} is the reflected power and P_{in} is the incident power, which will lead to similar results. The absorptance versus the frequency, computed by use of the proposed transmission-line model, is plotted in Fig. 1(b) (black line) at normal incident illumination ($\theta = 0°$) for a grating with dimensions $p = 10$ μm, $b = 0.6$ μm, and $d = 10$ μm loaded with graphene on top with a Fermi level of 0.3 eV. The trench width b is much smaller than the period p in all our designs, and the graphene can be placed over the grating without being bent at the corrugations.

To verify the accuracy of the equivalent-circuit model presented, we compute the response of the proposed structure by numerical simulations performed with COMSOL MULTIPHYSICS. The structure is again assumed to be infinite along the y direction in the numerical modeling case, as shown in Fig. 1(a), and is modeled as a 2D system to accelerate the calculations. Periodic boundary conditions are used in the x direction and port boundaries are placed in the z direction to create the incident plane wave. Graphene is modeled as a surface current, due to its planar (2D) nature, described as $J = \sigma_g E$, where E is the electric field along its surface and σ_g is the linear graphene conductivity given before by the Drude model.

The computed absorptances based on the theoretical method and the numerical methods are shown in Fig. 1(b) as black and blue lines, respectively, and are found to be in good agreement. The small frequency shift between theoretical and simulation results can be attributed to the approximation of gold with a PEC in the theoretical model, as well as the finite-size mesh used during the full-wave modeling. However, both results are very similar, and one pronounced perfect-absorption peak is demonstrated in Fig 1(b) at the resonance of the hybrid grating. At this resonant point, a magnetic plasmon mode is formed due to

the generation of highly localized magnetic fields inside the grating's trench accompanied by high electric fields that are expected to boost nonlinearities [15]. The electric-field-enhancement distribution along the structure at the resonant frequency is demonstrated in the right inset in Fig. 1(b) and is computed by our calculation of the ratio $|E/E_0|$, where E_0 represents the amplitude of the incident electric field. The electric field can be enhanced by approximately 19 times inside the grating's trench and, more importantly, along its surface, where graphene will be deposited. The perfect absorption obtained indicates a strong coupling and interference between the terahertz plasmons of graphene and the metallic grating. In addition, we calculate the absorptance of a plain metallic grating (i.e., without graphene on top of it) by using the same numerical method. The result is shown by the green line in Fig. 1(b). It is interesting that a substantial frequency blueshift is obtained when graphene is introduced over the grating. The addition of graphene will also lead to dynamic tunability of the absorption resonant frequency, as demonstrated later. When the polarization of the incident wave is switched and the magnetic field is oriented along the length of the grating [transverse electric (TE) polarization], no resonance is observed since both graphene and the metallic grating cannot support TE plasmons and, as a result, cannot couple to the incident TE radiation. We also verify that the absorptance of a flat gold substrate with and without graphene on top is very low because there is no plasmon formation along the flat interface [84].

Next we investigate the effect of the grating's geometry on the calculated perfect absorptance of the proposed hybrid graphene grating. Throughout this work and unless otherwise specified after this point, we always assume the following realistic graphene parameters: $E_F = 0.1$ eV, $\tau = 10^{-13}$ s, and the following practical-to-realize grating microscale dimensions: $p = 8$ μm, $d = 8$ μm, and $b = 0.6$ μm. Figure 2(a) displays a contour plot of the computed absorptance for TM-polarized plane waves impinging at normal incidence as a function of the frequency and period, where the grating's dimensions $d = 8$ μm and $b = 0.6$ μm have fixed values. Clearly, the absorptance remains strong as we vary the period p from 5 to 25 μm, indicating a strong coupling between the grating and graphene plasmons independent of the periodicity. We also verify that higher-order diffraction modes or surface waves are not excited by the proposed grating if the incident wave has frequencies in the currently used range of 6–12 THz. The resonant frequency of the perfect absorptance is slightly affected by the period, and the bandwidth of the resonance peak is decreased as the period is increased. The resonant frequency of the perfect absorptance is more sensitive to the height of the grating. It decreases as the grating height is increased, as illustrated in Fig. 2(b), where the computed absorptance is plotted as a function of the frequency and grating height. Thus,
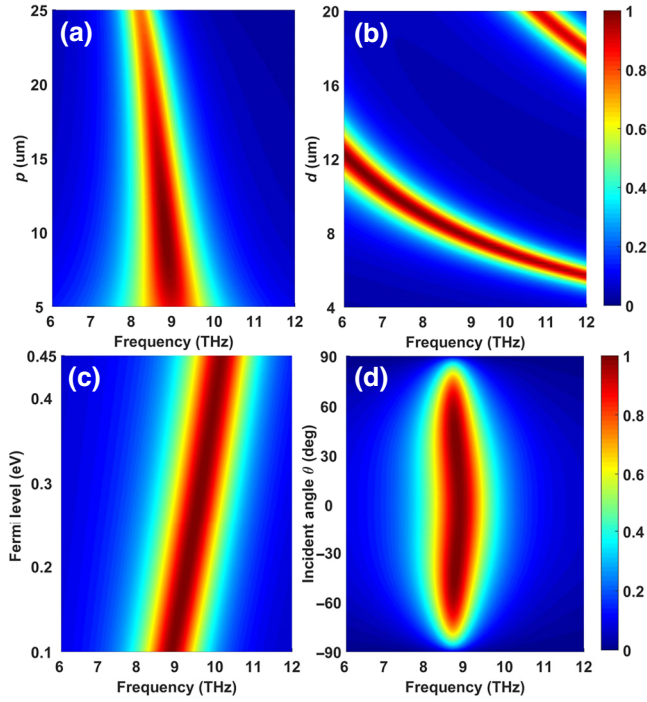
FIG. 2. Computed absorptance contour plots of the graphene-covered grating as a function of the frequency and (a) period p of the grating, (b) height d of the grating, (c) Fermi level of graphene, and (d) incident angle of the excitation wave.

it is possible to tune the perfect absorptance to different frequencies by variation of the grating geometry.

The perfect absorptance can also be tuned without change of the grating geometry but by electrostatic gating of the graphene, leading to a change in its doping level. The effect of different graphene Fermi levels on the perfect absorptance of the proposed graphene-covered gratings is demonstrated in Fig. 2(c). There is a substantial shift in the resonant frequency of the perfect absorptance as the Fermi level is increased. The modification of the Fermi level leads to different graphene properties and, as a result, to a frequency shift in the resonant response of the graphene plasmons. However, it is interesting that the absorptance remains perfect between 0.1 and 0.45 eV and only blueshifts as the doping level is increased. This doping variation can be achieved by electrostatic gating of the graphene monolayer with a pair of transparent electrodes, as explained in the next paragraph [85]. Finally, we investigate the performance of the proposed graphene-covered grating for different incident angles of the excitation wave. The calculated absorptance is shown in Fig. 2(d) as a function of the incident angle and frequency. Evidently, the absorptance remains almost perfect at the same resonant frequency over a wide range of incident angles, in particular between 80° and −80°.

The currently proposed structure can be realized with existing well-established fabrication methods, since just a

graphene monolayer needs to be deposited on a microscale metallic grating. The gating voltage can be applied only on the suspended part of the graphene sheet because the remaining graphene part will be shorted while touching the metallic grating. The portion of graphene along the grating ridges has no effect on the absorption and nonlinear response of the proposed hybrid structure. Hence, the nonuniform doping profile of graphene will not affect the response of the configuration presented. This is because only the suspended part of graphene over the trenches strongly interacts with the incident absorbed power, as clearly shown by the field and power profiles in Supplemental Material [84]. Surface waves are not excited along the grating ridges at the perfect-absorption frequency and only localized power is formed on the upper part of the trenches at this frequency, as depicted in Supplemental Material [84]. As a result, the fields along the trenches of the grating are the strongest [84], where the graphene monolayer is located. Thus, the nonlinear signal will be mainly generated by the strong fields interacting with graphene in these nanoregions. The metallic trenches can be loaded with a dielectric material to efficiently gate the suspended graphene sheet, leading to a voltage-controlled perfect absorber. The relationship between the Fermi level E_F and the gate voltage V_g for this gating configuration is $E_F = h v_F \sqrt{\pi C V_g / e}$ [86], where h is the Planck constant and $v_F = 1 \times 10^6$ m/s is the graphene Fermi velocity. The formed electrostatic capacitance per unit area C is given by $C = \varepsilon_0 \varepsilon_d / d$, where ε_d and d are the dielectric permittivity and thickness (height) of the grating trench, respectively. Here we assume $\varepsilon_d = 4.4$, and the highest gate voltage to achieve the maximum Fermi level (0.45 eV) used is computed to be 123 V, which is realistic and relatively low, paving the way toward potential experimental verification of the proposed tunable terahertz absorber [87].

III. THIRD-HARMONIC GENERATION

During the analysis presented in Sec. II, we proved that perfect and tunable absorption can be achieved by use of a hybrid metallic grating covered by graphene. It was demonstrated that the electric field is greatly enhanced at the absorption resonance due to the strong coupling between the graphene and the grating plasmonic responses. The increased light-matter interactions achieved by the proposed hybrid structure and obtained at the perfect-absorptance frequency have the potential to dramatically enhance the nonlinear response of graphene at low terahertz frequencies. Toward this goal, in this section, we investigate the THG efficiency of the proposed graphene-covered grating when all the nonlinear properties of the materials used are included in our nonlinear simulations. The fundamental frequency (FF) that excites the nonlinear system is always set to coincide with the perfect-absorptance resonant frequency of the proposed hybrid

structure. The strong electric fields at the resonance will subsequently boost the excited nonlinear effects.

Gold can be assumed to exhibit a PEC-like response at low terahertz frequencies, since it has very high conductivity and the fields minimally penetrate its bulk volume [88,89]. However, to ensure the accuracy of our nonlinear simulations, we include its nonlinear susceptibility $\chi^{(3)}_{Au} = 2.45 \times 10^{-19}$ m^2/V^2 in the infrared region [90], in addition to its linear Drude model, as described in Sec. II. Hence, the Kerr nonlinear permittivity of gold is given by $\varepsilon_{NL,Au} = \varepsilon_{L,Au} + \chi^{(3)}_{Au} E^2_{FF}$, where E_{FF} is the enhanced electric field induced at the FF and shown in the right inset in Fig. 1(b). We demonstrate later that the nonlinear response of the proposed system is dominated by the nonlinear properties of graphene and not the nonlinear permittivity of the gold grating.

The third-order nonlinear surface conductivity of graphene at terahertz frequencies is calculated by the formula [59]

$$\sigma^{(3)} = \frac{i\sigma_0 (\hbar v_F e)^2}{48\pi (\hbar\omega)^4} T\left(\frac{\hbar\omega}{2E_F}\right), \qquad (1)$$

where $\sigma_0 = e^2/4\hbar$, $v_F = 1 \times 10^6$ m/s, and $T(x) = 17 G(x) - 64G(2x) + 45G(3x)$, where $G(x) = \ln|(1+x)/ (1-x)| + i\pi\theta(|x| - 1)$, where $\theta(z)$ is the Heaviside step function. Graphene is modeled in COMSOL MULTIPHYSICS as a nonlinear surface current that can be expressed as $J = \sigma_g E_{TH} + \sigma^{(3)} E^3_{FF}$ [91], where E_{FF} and E_{TH} are the electric fields induced at the FF and the third harmonic (TH), respectively. An additional electromagnetic wave solver needs to be included in COMSOL MULTIPHYSICS and coupled to the FF solver to accurately compute the THG radiation, which will solve the nonlinear Maxwell equations at the TH frequency $\omega_{TH} = 3\omega$. The surface-current formalism used to model the nonlinear graphene leads to more-accurate simulation results combined with less-stringent mesh quality requirements. This type of simulation is faster and more accurate than the widely used conventional numerical three-dimensional graphene modeling, where graphene is considered to be a bulk material

[63]. The undepleted-pump approximation is used in all our nonlinear simulations, since the nonlinear signals are expected to be weaker than their linear counterparts.

The schematic of the THG process is illustrated in Fig. 3(a). In this case, a wave with frequency 3ω will be generated when an incident wave with FF ω excites the proposed nonlinear graphene-covered grating. The insets in Fig. 3(b) demonstrate the electric-field-enhancement distributions for this structure at the FF and the TH frequency, respectively. Clearly, enhanced localized electric fields are obtained both at the FF resonance and at the TH frequency. To take advantage of the strong field enhancement and boost THG, the frequency of the FF excitation wave is located close to the perfect-absorptance resonance, which is computed to be around 8.8 THz in this case. The proposed nonlinear structure is illuminated at normal incidence with a relatively low input intensity of 10 kW/cm^2. This value is substantially lower than intensities used in previous work based on just the nonlinear properties of graphene without the addition of plasmonic structures [27]. By our calculation of the integral $\int_C \vec{S} \cdot \vec{n}$ over the entire surface of the structure and at the far field [92], where $\vec{S}$ is the Poynting vector crossing the boundary surface C and $\vec{n}$ is the boundary norm vector, the radiated output power of the TH wave with radiation frequency $3f = 26.4$ THz is computed. We assume a fictitious large distance of 1 m for the y-direction length of the proposed structure in all our 2D simulations, and thus the output power is always computed in watts. The result for the radiated output power of the TH wave is shown in Fig. 3(b). There is a peak at the TH radiation around the absorption resonance, which coincides with the FF, and its maximum value can reach 1.6 W. In addition, the TH radiation power shown in Fig. 3(b) follows the same trend as the absorptance shown in Fig. 1(b). Finally, we stress that reflected waves do not exist at the fundamental frequency $f = 8.8$ THz due to the high absorptance of the proposed hybrid grating but there are strong THG reflected waves due to low absorptance at the third-harmonic frequency $3f = 26.4$ THz.

Next we compute the THG conversion efficiency (C_{eff}), which is a suitable metric to describe the THG power
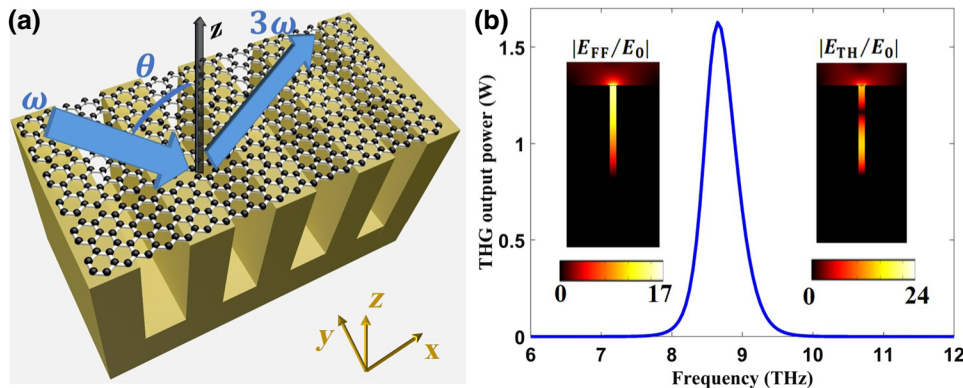

FIG. 3. (a) The THG process due to the nonlinear graphene-covered grating. (b) The computed output power of the THG wave as a function of the incident-wave fundamental frequency. The insets show the computed electric-field-enhancement distributions at the FF of 8.8 THz (left inset) and the TH frequency of 26.4 THz (right inset).
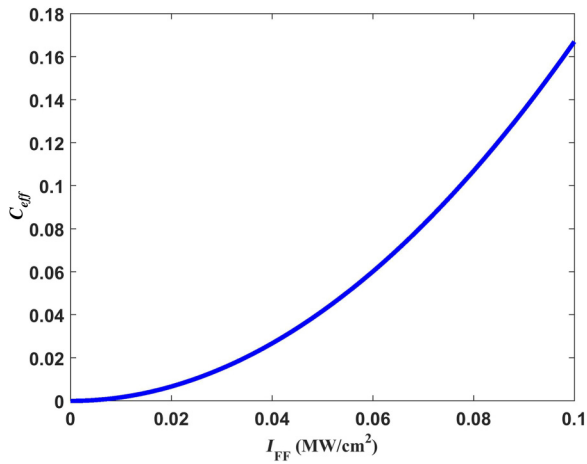
FIG. 4. Computed THG C_{eff} on a linear scale as a function of the intensity of the incident FF wave. Relatively low intensities of the incident FF terahertz wave lead to very high THG C_{eff}.
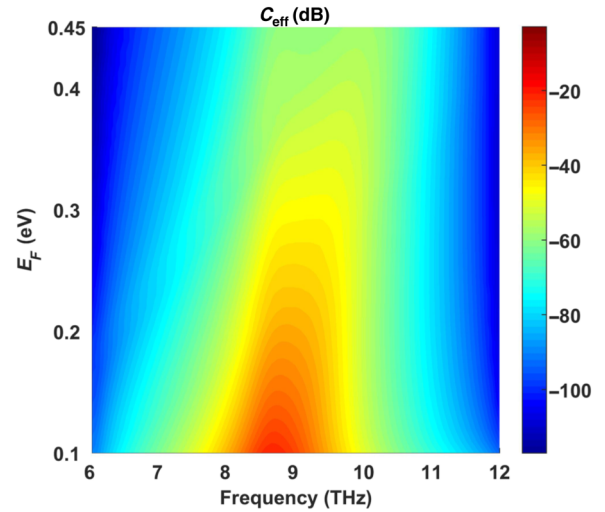

FIG. 5. The computed THG C_{eff} on a logarithmic scale at normal incidence as a function of the fundamental frequency and graphene's Fermi level of the proposed nonlinear hybrid graphene-covered grating.

strength in a more-quantitative way. It is defined as the ratio of the radiated THG power outflow $P_{\text{out,TH}}$ to the input FF power $P_{\text{in,FF}}$: $C_{\text{eff}} = P_{\text{out,TH}}/P_{\text{in,FF}}$ [93]. It is clear that the intensity of the incident FF wave plays a key role in the C_{eff}. The C_{eff} is plotted on a linear scale as a function of the intensity of the FF wave in Fig. 4. The FF is fixed at 8.8 THz, where the maximum linear absorption is achieved for the currently used geometrical parameters $p = 8$ μm, $b = 0.6$ μm, and $d = 8$ μm. The C_{eff} is dramatically enhanced by our increasing the intensity of the incident FF wave. Notably, the C_{eff} can reach high values (16%) with very low input intensities (100 kW/cm²), which is a substantial improvement compared with the previously proposed strong THG obtained by patterned nonlinear graphene metasurfaces at similar terahertz frequencies [94]. It is even more interesting that this high efficiency can be achieved by the currently proposed more-realistic and easy-to-fabricate configuration. In the proposed structure, a graphene monolayer is used to obtain a strong nonlinear response instead of patterned graphene microribbons, which can suffer from detrimental edge-loss effects at their discontinuities and other fabrication imperfections. The input intensities used have realistic values and even-higher terahertz-radiation intensities on the order of several megawatts per square centimeter have been reported in previous work with specialized configurations [95,96]. We stress that the THG efficiencies presented are on the order of a few percent and these values are higher than those for most nonlinear plasmonic devices presented so far [38]. The relationship between the computed C_{eff} and the input intensity has a quadratic shape (Fig. 4), as expected for THG nonlinear conversion efficiency. The input intensity of the FF wave is fixed to the low value of 20 kW/cm² in all the following calculations unless otherwise specified.

According to Eq. (1), it is expected that a stronger nonlinear response will be obtained by use of a lower Fermi level (i.e., less-doped graphene). The THG C_{eff} will also be affected by the FF since the nonlinear surface conductivity of graphene given by Eq. (1) is inversely proportional to ω. As a consequence, a stronger nonlinear response and higher C_{eff} are expected to be achieved at lower terahertz frequencies. However, the enhanced electric fields at the FF resonance will also affect the THG process. To verify how the THG C_{eff} will be affected by all these different parameters, the C_{eff} of the proposed nonlinear structure is computed by our sweeping of the graphene Fermi level and the fundamental frequency. The resulting contour plot is shown in Fig. 5. Clearly, the THG C_{eff} decreases as the Fermi level is increased or in the case of off-resonance operation. The maximum C_{eff} is obtained for $f_{\text{FF}} \approx 8.8$ THz and slightly doped graphene with $E_F = 0.1$ eV. This trend is consistent with the absorptance analysis reported in Sec. II. It is interesting that low-doped graphene, which is easier to produce, can lead to enhanced nonlinear effects with the proposed configuration.

We discussed in Sec. II the effect of the proposed hybrid structure's geometry on the linear-absorption spectrum. In this section, we investigate the effect of the geometry on the THG nonlinear process. Toward this goal, the THG C_{eff} is computed by our sweeping of the FF and the period or height of the grating, as shown in Figs. 6(a) and 6(b), respectively. The C_{eff} (plotted in decibels) is tunable and follows the same trend as the linear absorptance enhancement illustrated in Figs. 2(a) and 2(b). When the FF is tuned around the resonant frequency, a noticeable enhancement in the THG CE is observed for every period or height of the plasmonic grating, with results shown in Fig. 6. This
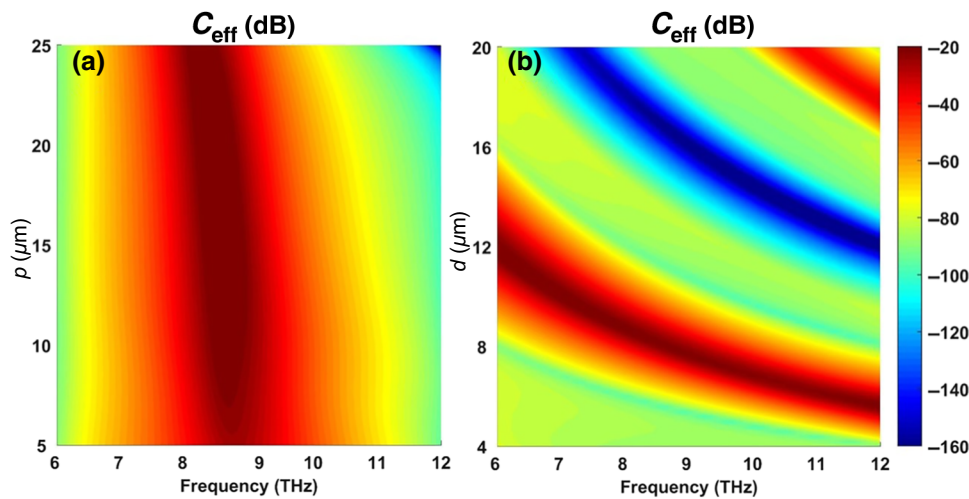
FIG. 6. THG-C_{eff} contour plots of the proposed nonlinear hybrid structure at normal incidence as a function of the frequency and (a) the period and (b) the height of the grating. The grating height is fixed to $d = 8$ μm in (a) and the period is fixed to $p = 8$ μm in (b).

is directly related to the enhancement of the electric field at the absorption resonance peak that boosts the nonlinear response of the structure, translating to enhanced C_{eff}. In all the simulations described above, we set the intensity of the illuminating wave to very low values (20 kW/cm^2), where the THG C_{eff} is relatively high and equal to -22 dB at the resonance. Hence, it is possible to also tune the THG nonlinear waves by change of the plasmonic grating's geometrical parameters and without alteration of the graphene properties. There is no special requirement in the fabrication of the graphene monolayer used in the proposed hybrid structure since different graphene relaxation times are found not to affect the absorptance and THG conversion efficiency. We provide more details about this advantageous feature for practical implementation in Supplemental Material [84].

Finally, the TH output power is computed with and without the graphene monolayer to prove that the addition of graphene is crucial to obtain enhanced nonlinear effects. The comparison results for the proposed hybrid structure and a similar structure made of a flat metallic substrate (no grating; geometry shown in the inset in Fig. 7) with and without graphene on top are plotted in Fig. 7. For a fair comparison, all the results are obtained under a varying incident angle wave and by use of the same fundamental frequency of 8.8 THz. Moreover, the grating height and the substrate thickness are also kept identical during this comparison. The TH output power of the proposed graphene-covered hybrid grating (blue line in Fig. 7) is by far the highest compared with all the other scenarios: (i) the plasmonic grating with the same dimensions but without graphene on top (black line in Fig. 7), (ii) the graphene-covered flat metallic substrate without the grating corrugations (green line in Fig. 7), and (iii) the flat metallic substrate without the graphene monolayer on top (red line in Fig. 7). Under normal incidence, the TH radiation generated by the proposed graphene-covered plasmonic grating has an impressive 28-orders-of-magnitude THG

enhancement compared with the same plasmonic grating but without graphene. In a similar way, the flat metallic substrate produces much-higher-intensity TH radiation when graphene is placed on top of it, but the intensity is still much lower than in the plasmonic grating case. Thus, it can be concluded that graphene plays a crucial role in the strong enhancement of the THG process. The same structure without the key nonlinear element of graphene will not produce such significant THG radiation. These results directly demonstrate the great potential of graphene in terahertz nonlinear optics. In addition, the THG process is much stronger in the case of the plasmonic grating
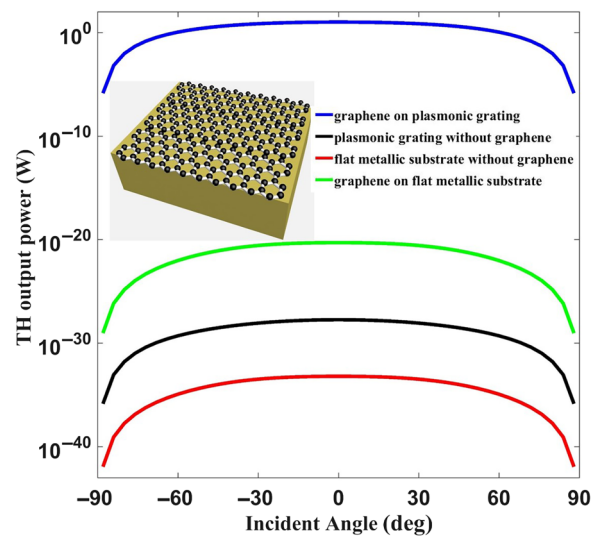

FIG. 7. Comparison of the TH output power of the proposed hybrid graphene-covered grating (blue line), the plasmonic grating without graphene (black line), the flat metallic substrate covered with graphene (green line; geometry shown in the inset), and the flat metallic substrate without graphene (red line). All the structures are excited by an 8.8-THz incident wave under various incident angles.

configuration compared with the flat metallic substrate without corrugations since the grating structure can enable strong localized electric fields at its plasmonic resonance that strongly couple to graphene, as mentioned before. The THG output power remains relative insensitive across a broad incident angle range, especially between $-30°$ and $30°$, in agreement with the linear-absorption spectrum.

IV. FOUR-WAVE MIXING

Another interesting third-order nonlinear optical process is FWM, which typical requires very high input intensities. A feasible way to increase the efficiency of FWM is to increase the local field intensity at both input waves by use of an artificially engineered structure [39,97]. In the following, we demonstrate that the proposed graphene-covered grating can serve as an excellent platform to boost this nonlinear process at terahertz frequencies. The strong coupling and interference between the plasmonic resonance of the metallic grating and the terahertz surface plasmons along the graphene monolayer can lead to strong local field enhancement, as demonstrated before, which is expected to enhance FWM. In FWM, two photons with frequency ω_1 and one photon with frequency ω_2 are mixed and a photon is emitted with frequency $\omega_3 = 2\omega_1 - \omega_2$. To take advantage of the strong field enhancement at the resonance and boost the FWM process, the two incident-wave frequencies are chosen to be $f_1 = 8.8$ THz and $f_2 = 9.2$ THz. Thus, the FWM wave generated will be at $f_3 = 8.4$ THz. The frequencies of the incident and generated waves are all very close to the maximum-absorptance resonant frequency (8.8 THz). Hence, the electric fields induced by the incident and generated waves are expected to be greatly enhanced at these frequencies. The computed electric-field-distribution enhancement at the generated FWM frequency $f_3 = 8.4$ THz is demonstrated in the inset in Fig. 8(b).

Again, we use COMSOL MULTIPHYSICS to investigate the enhanced FWM nonlinear process based on the proposed nonlinear graphene-covered grating. A schematic of this nonlinear procedure is illustrated in Fig. 8(a). The boundary conditions are the same as for the THG simulations presented before except that one more electromagnetic wave solver is required to take into account the mixing mechanism introduced by the additional ω_2 input wave. Both incident waves are TM polarized and have incident angles θ_1 and θ_2, respectively. In addition, both input intensities are selected to have low values of 20 kW/cm^2. We measure the FWM radiated power through the upper boundary of the simulation domain by integrating the power outflow over the surface that surrounds the nonlinear structure, as was done before in the case of THG. The computed FWM output results are shown in Fig. 8(b). The incident angle θ_2 is kept constant and equal to zero, and the incident angle θ_1 varies from $0°$ to $\pm 90°$. The maximum output power is 381 W at $\theta_1 = 0°$ and remains close to this peak value within a relatively broad range of incident angles ($-30°$ to $30°$). The FWM output power is symmetric with respect to θ_1 and relatively insensitive to this incident angle. The same result is obtained when the incident angles θ_1 and θ_2 of both input waves are simultaneously swept. The computed contour plot is shown in Fig. 9. In this case, the incident frequencies used are the same as for the case presented in Fig. 8(b). It can be concluded that the FWM efficiency of the proposed graphene-covered grating is very high and relatively insensitive to the excitation angles of both incident waves.

The FWM efficiency can be calculated by computation of the ratio $P_{\text{out,tot}}/P_{\text{in,tot}}$, where $P_{\text{out,tot}}$ and $P_{\text{in,tot}}$ are the total output and input powers, respectively. It is noteworthy that the FWM efficiency of the proposed hybrid grating can reach very high values of approximately 12% with a relatively low input intensity of 20 kW/cm^2. Such high nonlinear efficiency has never been reported before in the literature for both theoretical and experimental nonlinear plasmonic devices [38]. This efficiency is even higher than that of THG presented before because one more incident wave is contributing its power in the FWM process. The high nonlinear efficiency obtained is one of the major advantages of the proposed hybrid terahertz nonlinear graphene-plasmonic configuration. The FWM
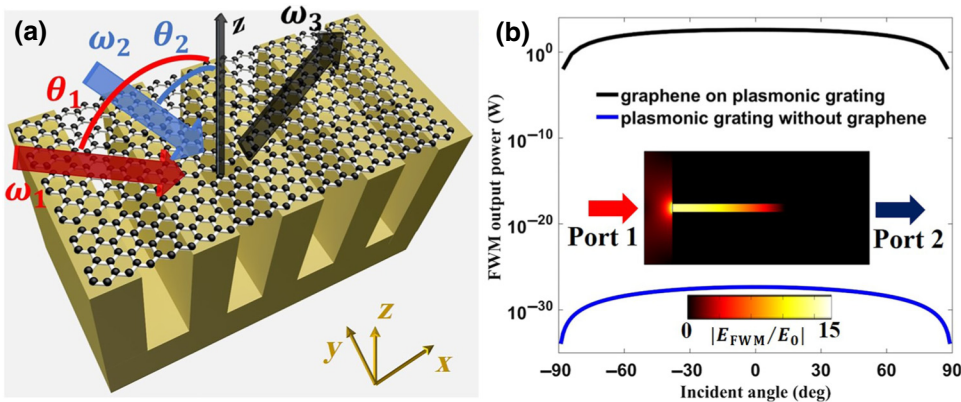

FIG. 8. (a) The FWM process due to the nonlinear graphene-covered plasmonic grating. (b) Computed output power of the generated FWM wave ω_3 as a function the excitation angle θ_1 of the incident wave for the cases of the graphene-covered grating (black line) and the grating without the graphene monolayer (blue line). The inset shows the computed electric-field-enhancement distribution at the FWM frequency $f_3 = 8.4$ THz.
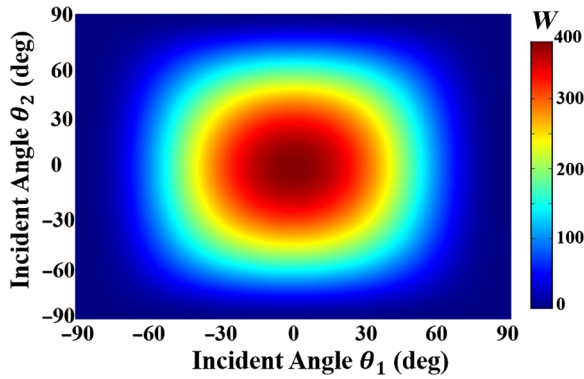
FIG. 9. Computed output power of the generated FWM wave as a function of the excitation angles of both incident waves impinging on the nonlinear hybrid graphene-covered grating.

output power generated by the metallic grating without graphene on top is also calculated and is plotted in Fig. 8(b) (blue line). Clearly, the FWM output power is dramatically increased with the proposed graphene-covered grating by approximately 25 orders of magnitude compared with a plain grating without graphene. This comparison provides additional proof of the key contribution of graphene in the boosted nonlinear response of the proposed plasmonic system.

As indicated in Sec. III, the Fermi level E_F will have a pronounced effect on the nonlinear response of the proposed structure. It will lead to different values of the nonlinear conductivity of graphene, which is given by Eq. (1). This effect is also predominant in the FWM process. The variation of the FWM output power due to increased E_F is computed and shown in Fig. 10(a). The incident frequencies are again fixed to $f_1 = 8.8$ THz and $f_2 = 9.2$ THz in this case. The FWM output power is decreased by 5 orders of magnitude when the Fermi level is increased from 0.1 to 0.45 eV. This trend is consistent with the formula for the third-order nonlinear surface conductivity of graphene

given by Eq. (1). Moreover, we explore the effect of the proposed hybrid structure's geometry on the FWM process, similarly to our previous THG analysis. The results are shown in Figs. 10(b) and 10(c). The FWM output power is relatively high when the period varies from 5 to 25 μm, and reaches a maximum value of 1150 W for a period of approximately 15 μm. This trend is similar to that of the THG-C_{eff} contour plot shown in Fig. 6(a), where the FF wave is fixed to 8.8 THz. The FWM output power changes dramatically with the grating's height, as demonstrated in Fig. 10(c). It reaches a maximum value of 382 W for $d = 8$ μm and a minimum value of 2×10^{-11} W for $d = 16$ μm. This trend is again similar to that of the THG-CE contour plot shown in Fig. 6(b). The absorption resonant frequency is strongly shifted when we change the grating height d [see Fig. 2(b)] and this leads to a dramatic variation in the FWM output power. Thus, it can be concluded that the output radiated power of the generated FWM wave can be tuned by our either changing of the graphene's Fermi level or the geometry of the proposed hybrid structure.

Finally, an alternative robust way to control the output radiation power of the generated FWM wave is achieved by our varying of the incident power of both excitation waves. The FWM signal is expected to follow a square-power-law relation as a function of the input power P_1 of the first incident wave ω_1 and a linear-power-law relation as a function of the input power P_2 of the second incident wave ω_2 [33]. The effect of the input pump intensities P_1 and P_2 of the two incident waves with frequencies of $f_1 = 8.8$ THz and $f_2 = 9.2$ THz, respectively, on the output power of the generated FWM wave is illustrated in Fig. 11. The generated FWM power is approximately a square function of P_1 and a linear function of P_2. This result also demonstrates that P_1 has a stronger effect on the generated FWM power [39]. Hence, the generated FWM power can be the further enhanced by increase of the input power of both incident waves. Thermal damage to the gold
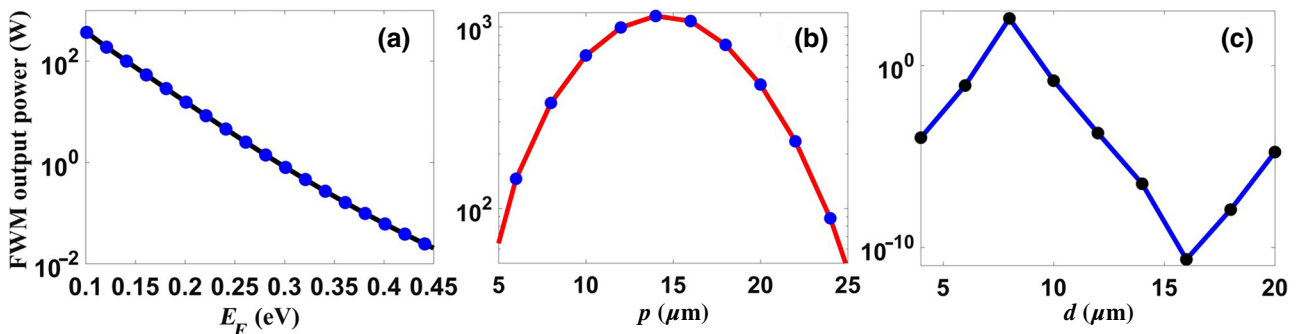

FIG. 10. Computed output power of the FWM wave generated by the nonlinear hybrid graphene-covered grating [schematically depicted in Fig. 8(a)] as a function of (a) graphene's Fermi level with fixed structure dimensions of $p = 8$ μm, $b = 0.6$ μm, and $d = 8$ μm, (b) the grating period p when $E_F = 0.1$ eV and the other dimensions are fixed at $b = 0.6$ μm and $d = 8$ μm, and (c) the grating height d when $E_F = 0.1$ eV and the other dimensions are fixed at $b = 0.6$ μm and $p = 8$ μm.
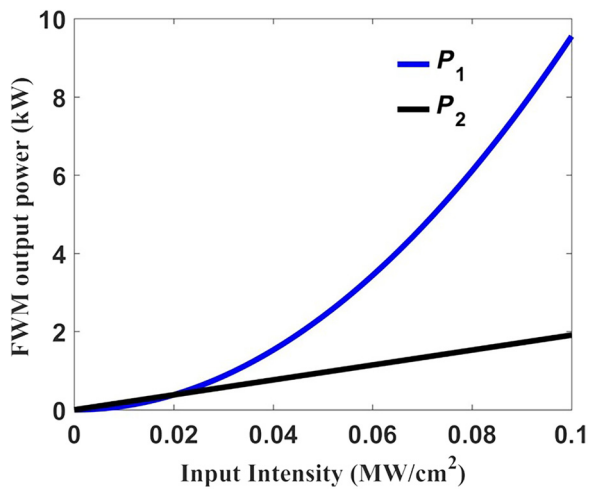
FIG. 11. The effect of the input pump intensities P_1 and P_2 on the output power of the generated FWM wave. The pump frequencies of the two incident waves are $f_1 = 8.8$ THz and $f_2 = 9.2$ THz.

grating can occur only for very high input intensities on the order of gigawatts per square centimeter. In addition, graphene has a higher melting point than gold and is not expected to be affected by thermal effects.

V. CONCLUSIONS

In this work, we analyze and demonstrate enhanced nonlinear terahertz effects on the basis of a hybrid terahertz planar nonlinear device composed of a graphene monolayer placed over a metallic grating. The strong nonlinear response presented is mainly due to the localization and enhancement of the electric field at the absorption resonance of the proposed structure and the large nonlinear conductivity of graphene at low terahertz frequencies. It is demonstrated that the efficiency of the THG and FWM nonlinear processes can be dramatically enhanced by many orders of magnitude with the proposed device compared with conventional nonhybrid metallic gratings and substrates. The nonlinear efficiencies presented are computed to be very large, on the order of a few percent. They are higher than for most of the state-of-the-art nonlinear planar plasmonic devices. Another major advantage of the proposed hybrid terahertz nonlinear configuration is that its nonlinear response can be dynamically tuned by different mechanisms. In particular, the output powers of the THG and FWM processes can be tuned by variation of the metallic grating dimensions. This is because the geometrical variations can lead to significant shifts in the absorption resonant frequency, where the electric field, which triggers the nonlinear response, is greatly enhanced. Even more importantly, the nonlinear response can be dynamically modulated without alteration of the geometry of the

proposed device and just by variation of the graphene doping level. Finally, we demonstrate that the efficiencies of the THG and FWM processes can be further increased by increasing the input intensity of the incident waves.

The proposed graphene-covered metallic gratings can be realized with commonly used fabrication techniques. They can be built by a combination of chemical vapor deposition to efficiently exfoliate graphene and the deposition of a graphene monolayer over a microscale gold grating, which can be constructed by conventional lithography techniques. The optimized grating design presented usually requires a relatively high aspect ratio (groove depth d to groove width b) with values between 10 and 20 to achieve strong absorption and a nonlinear response, but similar metallic gratings have recently been built by photolithography [98], a deep-reactive-ion-etching Bosch process [99], or nanoimprint lithography [100]. The proposed hybrid nonlinear graphene-plasmonic devices are envisioned to have several applications relevant to the new field of nonlinear optics based on 2D materials. They can be used in the design of terahertz-frequency generators, all-optical signal processors, and wave mixers. Moreover, they are expected to be valuable components in the design of new nonlinear-terahertz-spectroscopy and noninvasive-terahertz-subwavelength-imaging devices. Finally, the strong field confinement inside the nanoscale trenches and along graphene, achieved by the proposed hybrid grating, can be used to enhance dipole-forbidden transitions on the atomic scale [101,102].

[1] K. S. Novoselov, V. I. Fal'ko, L. Colombo, P. R. Gellert, M. G. Schwab, and K. Kim, A roadmap for graphene, Nature (London) **490**, 192 (2012).

[2] Q. Bao and K. P. Loh, Graphene photonics, plasmonics, and broadband optoelectronic devices, ACS Nano **6**, 3677 (2012).

[3] F. H. L. Koppens, D. E. Chang, and F. J. García de Abajo, Graphene plasmonics: A platform for strong light–matter interactions, Nano Lett. **11**, 3370 (2011).

[4] P.-Y. Chen, C. Argyropoulos, M. Farhat, and J. S. Gomez-Diaz, Flatland plasmonics and nanophotonics based on graphene and beyond, Nanophotonics **6**, 1239 (2017).

[5] A. N. Grigorenko, M. Polini, and K. S. Novoselov, Graphene plasmonics, Nat. Photonics **6**, 749 (2012).

[6] T. Guo and C. Argyropoulos, Broadband polarizers based on graphene metasurfaces, Opt. Lett. **41**, 5592 (2016).

[7] P.-Y. Chen and A. Alù, Atomically thin surface cloak using graphene monolayers, ACS Nano **5**, 5855 (2011).

[8] P.-Y. Chen, C. Argyropoulos, and A. Alu, Terahertz antenna phase shifters using integrally-gated graphene transmission-lines, IEEE Trans. Antennas Propag. **61,** 1528 (2013).

[9] C. Argyropoulos, Enhanced transmission modulation based on dielectric metasurfaces loaded with graphene, Opt. Express **23,** 23787 (2015).

[10] A. Khavasi, Design of ultra-broadband graphene absorber using circuit theory, J. Opt. Soc. Am. B **32,** 1941 (2015).

[11] F. Bonaccorso, Z. Sun, T. Hasan, and A. C. Ferrari, Graphene photonics and optoelectronics, Nat. Photonics **4,** 611 (2010).

[12] S. Thongrattanasiri, F. H. L. Koppens, and F. J. García de Abajo, Complete Optical Absorption in Periodically Patterned Graphene, Phys. Rev. Lett. **108,** 047401 (2012).

[13] H. Yan, X. Li, B. Chandra, G. Tulevski, Y. Wu, M. Freitag, W. Zhu, P. Avouris, and F. Xia, Tunable infrared plasmonic devices using graphene/insulator stacks, Nat. Nanotechnol. **7,** 330 (2012).

[14] M. Furchi, A. Urich, A. Pospischil, G. Lilley, K. Unterrainer, H. Detz, P. Klang, A. M. Andrews, W. Schrenk, G. Strasser, and T. Mueller, Microcavity-integrated graphene photodetector, Nano Lett. **12,** 2773 (2012).

[15] B. Zhao, J. M. Zhao, and Z. M. Zhang, Enhancement of near-infrared absorption in graphene with metal gratings, Appl. Phys. Lett. **105,** 031905 (2014).

[16] D. Ansell, I. P. Radko, Z. Han, F. J. Rodriguez, S. I. Bozhevolnyi, and A. N. Grigorenko, Hybrid graphene plasmonic waveguide modulators, Nat. Commun. **6,** 8846 (2015).

[17] S. A. Mikhailov and K. Ziegler, Nonlinear electromagnetic response of graphene: Frequency multiplication and the self-consistent-field effects, J. Phys. Condens. Matter **20,** 384204 (2008).

[18] K. L. Ishikawa, Nonlinear optical response of graphene in time domain, Phys. Rev. B **82,** 201402 (2010).

[19] M. M. Glazov, Second harmonic generation in graphene, JETP Lett. **93,** 366 (2011).

[20] K. Yang, S. Arezoomandan, and B. Sensale-Rodriguez, The linear and non-linear THz properties of graphene, Terahertz Sci. Technol. **6,** 223 (2013).

[21] M. M. Glazov and S. D. Ganichev, High frequency electric field induced nonlinear effects in graphene, Phys. Rep. **535,** 101 (2014).

[22] E. Hendry, P. J. Hale, J. Moger, A. K. Savchenko, and S. A. Mikhailov, Coherent Nonlinear Optical Response of Graphene, Phys. Rev. Lett. **105,** 097401 (2010).

[23] J. A. Armstrong, N. Bloembergen, J. Ducuing, and P. S. Pershan, Interactions between light waves in a nonlinear dielectric, Phys. Rev. **127,** 1918 (1962).

[24] J. A. Squier, M. Müller, G. J. Brakenhoff, and K. R. Wilson, Third harmonic generation microscopy, Opt. Express **3,** 315 (1998).

[25] M. Mesch, B. Metzger, M. Hentschel, and H. Giessen, Nonlinear plasmonic sensing, Nano Lett. **16,** 3155 (2016).

[26] S.-Y. Hong, J. I. Dadap, N. Petrone, P.-C. Yeh, J. Hone, and R. M. Osgood, Optical third-harmonic generation in graphene, Phys. Rev. X **3,** 021014 (2013).

[27] N. Kumar, J. Kumar, C. Gerstenkorn, R. Wang, H.-Y. Chiu, A. L. Smirl, and H. Zhao, Third harmonic generation in graphene and few-layer graphite films, Phys. Rev. B **87,** 121406 (2013).

[28] N. L. Rangel, A. Gimenez, A. Sinitskii, and J. M. Seminario, Graphene signal mixer for sensing applications, J. Phys. Chem. C **115,** 12128 (2011).

[29] W. Min, S. Lu, M. Rueckel, G. R. Holtom, and X. S. Xie, Near-degenerate four-wave-mixing microscopy, Nano Lett. **9,** 2423 (2009).

[30] R. Salem, M. A. Foster, A. C. Turner, D. F. Geraghty, M. Lipson, and A. L. Gaeta, Signal regeneration using low-power four-wave mixing on silicon chip, Nat. Photonics **2,** 35 (2008).

[31] V. Boyer, A. M. Marino, R. C. Pooser, and P. D. Lett, Entangled images from four-wave mixing, Science **321,** 544 (2008).

[32] T. Yajima and H. Souma, Study of ultra-fast relaxation processes by resonant Rayleigh-type optical mixing. I. Theory, Phys. Rev. A **17,** 309 (1978).

[33] Y. Zhang, F. Wen, Y.-R. Zhen, P. Nordlander, and N. J. Halas, Coherent Fano resonances in a plasmonic nanocluster enhance optical four-wave mixing, Proc. Natl. Acad. Sci. **110,** 9215 (2013).

[34] A. Autere, H. Jussila, Y. Dai, Y. Wang, H. Lipsanen, and Z. Sun, Nonlinear optics with 2D layered materials, Adv. Mater., 1705963 (2018).

[35] J. R. M. Saavedra and F. J. García de Abajo, Enhanced graphene nonlinear response through geometrical plasmon focusing, Appl. Phys. Lett. **112,** 061107 (2018).

[36] R. W. Boyd, *Nonlinear Optics* (Academic Press, New York, 2003).

[37] M. Tonouchi, Cutting-edge terahertz technology, Nat. Photonics **1,** 97 (2007).

[38] M. Kauranen and A. V. Zayats, Nonlinear plasmonics, Nat. Photonics **6,** 737 (2012).

[39] B. Jin and C. Argyropoulos, Enhanced four-wave mixing with nonlinear plasmonic metasurfaces, Sci. Rep. **6,** 28746 (2016).

[40] J. Lee, M. Tymchenko, C. Argyropoulos, P.-Y. Chen, F. Lu, F. Demmerle, G. Boehm, M.-C. Amann, A. Alù, and M. A. Belkin, Giant nonlinear response from plasmonic metasurfaces coupled to intersubband transitions, Nature (London) **511,** 65 (2014).

[41] P.-Y. Chen, C. Argyropoulos, and A. Alù, Enhanced nonlinearities using plasmonic nanoantennas, Nanophotonics **1,** 221 (2012).

[42] C. Argyropoulos, P.-Y. Chen, G. D'Aguanno, and A. Alù, Temporal soliton excitation in an ϵ-near-zero plasmonic metamaterial, Opt. Lett. **39,** 5566 (2014).

[43] C. Argyropoulos, G. D'Aguanno, and A. Alù, Giant second-harmonic generation efficiency and ideal phase matching with a double ϵ-near-zero cross-slit metamaterial, Phys. Rev. B **89,** 235401 (2014).

[44] C. Argyropoulos, P.-Y. Chen, G. D'Aguanno, N. Engheta, and A. Alù, Boosting optical nonlinearities in ϵ-near-zero plasmonic channels, Phys. Rev. B **85,** 045129 (2012).

[45] Z. Huang, A. Baron, S. Larouche, C. Argyropoulos, and D. R. Smith, Optical bistability with film-coupled metasurfaces, Opt. Lett. **40,** 5638 (2015).

[46] C. Argyropoulos, C. Ciracì, and D. R. Smith, Enhanced optical bistability with film-coupled plasmonic nanocubes, Appl. Phys. Lett. **104,** 063108 (2014).

[47] C. Argyropoulos, P.-Y. Chen, F. Monticone, G. D'Aguanno, and A. Alù, Nonlinear Plasmonic Cloaks to Realize Giant All-Optical Scattering Switching, Phys. Rev. Lett. **108,** 263905 (2012).

[48] G. A. Wurtz, R. Pollard, W. Hendren, G. P. Wiederrecht, D. J. Gosztola, V. A. Podolskiy, and A. V. Zayats, Designed ultrafast optical nonlinearity in a plasmonic nanorod metamaterial enhanced by nonlocality, Nat. Nanotechnol. **6,** 107 (2011).

[49] R. Czaplicki, H. Husu, R. Siikanen, J. Mäkitalo, M. Kauranen, J. Laukkanen, J. Lehtolahti, and M. Kuittinen, Enhancement of Second-Harmonic Generation from Metal Nanoparticles by Passive Elements, Phys. Rev. Lett. **110,** 093902 (2013).

[50] M. Celebrano, X. Wu, M. Baselli, S. Großmann, P. Biagioni, A. Locatelli, C. De Angelis, G. Cerullo, R. Osellame, B. Hecht, L. Duò, F. Ciccacci, and M. Finazzi, Mode matching in multiresonant plasmonic nanoantennas for enhanced second harmonic generation, Nat. Nanotechnol. **10,** 412 (2015).

[51] K.-Y. Yang, R. Verre, J. Butet, C. Yan, T. J. Antosiewicz, M. Käll, and O. J. F. Martin, Wavevector-selective nonlinear plasmonic metasurfaces, Nano Lett. **17,** 5258 (2017).

[52] F. Walter, G. Li, C. Meier, S. Zhang, and T. Zentgraf, Ultrathin nonlinear metasurface for optical image encoding, Nano Lett. **17,** 3171 (2017).

[53] B. Zhao and Z. M. Zhang, Strong plasmonic coupling between graphene ribbon array and metal gratings, ACS Photonics **2,** 1611 (2015).

[54] A. V. Zayats and I. I. Smolyaninov, Near-field photonics: Surface plasmon polaritons and localized surface plasmons, J. Opt. A Pure Appl. Opt. **5,** S16 (2003).

[55] L. Wen, F. Sun, and Q. Chen, Cascading metallic gratings for broadband absorption enhancement in ultrathin plasmonic solar cells, Appl. Phys. Lett. **104,** 151106 (2014).

[56] Y. Cai, J. Zhu, and Q. H. Liu, Tunable enhanced optical absorption of graphene using plasmonic perfect absorbers, Appl. Phys. Lett. **106,** 043105 (2015).

[57] K. Aydin, V. E. Ferry, R. M. Briggs, and H. A. Atwater, Broadband polarization-independent resonant light absorption using ultrathin plasmonic super absorbers, Nat. Commun. **2,** 517 (2011).

[58] M. Tokman, X. Yao, and A. Belyanin, Generation of Entangled Photons in Graphene in a Strong Magnetic Field, Phys. Rev. Lett. **110,** 077404 (2014).

[59] J. L. Cheng, N. Vermeulen, and J. E. Sipe, Third order optical nonlinearity of graphene, New J. Phys. **16,** 053014 (2014).

[60] M. Gullans, D. E. Chang, F. H. L. Koppens, F. J. G. de Abajo, and M. D. Lukin, Single-Photon Nonlinear Optics with Graphene Plasmons, Phys. Rev. Lett. **111,** 247401 (2013).

[61] X. Yao, M. Tokman, and A. Belyanin, Efficient Nonlinear Generation of THz Plasmons in Graphene and Topological Insulators, Phys. Rev. Lett. **112,** 055501 (2014).

[62] J. D. Cox and F. J. G. De Abajo, Electrically tunable nonlinear plasmonics in graphene nanoislands, Nat. Commun. **5,** 5725 (2015).

[63] M. Weismann and N. C. Panoiu, Theoretical and computational analysis of second- and third-harmonic generation in periodically patterned graphene and transition-metal dichalcogenide monolayers, Phys. Rev. B **94,** 035435 (2016).

[64] D. A. Smirnova, A. E. Miroshnichenko, Y. S. Kivshar, and A. B. Khanikaev, Tunable nonlinear graphene metasurfaces, Phys. Rev. B **92,** 161406 (2015).

[65] X. Li, C. W. Magnuson, A. Venugopal, R. M. Tromp, J. B. Hannon, E. M. Vogel, L. Colombo, and R. S. Ruoff, Large-area graphene single crystals grown by low-pressure chemical vapor deposition of methane on copper, J. Am. Chem. Soc. **133,** 2816 (2011).

[66] M. Kahl, E. Voges, S. Kostrewa, C. Viets, and W. Hill, Periodically structured metallic substrates for SERS, Sens. Actuators B Chem. **51,** 285 (1998).

[67] L. Ju, B. Geng, J. Horng, C. Girit, M. Martin, Z. Hao, H. A. Bechtel, X. Liang, A. Zettl, Y. R. Shen, and F. Wang, Graphene plasmonics for tunable terahertz metamaterials, Nat. Nanotechnol. **6,** 630 (2011).

[68] P. B. Johnson and R. W. Christy, Optical constants of the noble metals, Phys. Rev. B **6,** 4370 (1972).

[69] A. Pors, E. Moreno, L. Martin-Moreno, J. B. Pendry, and F. J. Garcia-Vidal, Localized Spoof Plasmons Arise While Texturing Closed Surfaces, Phys. Rev. Lett. **108,** 223905 (2012).

[70] M. Jablan, H. Buljan, and M. Soljačić, Plasmonics in graphene at infrared frequencies, Phys. Rev. B **80,** 245435 (2009).

[71] Z. Li, K. Yao, F. Xia, S. Shen, J. Tian, and Y. Liu, Graphene plasmonic metasurfaces to steer infrared light, Sci. Rep. **5,** 12423 (2015).

[72] A. Gorbach, Graphene plasmonic waveguides for mid-Infrared supercontinuum generation on a chip, Photonics **2,** 825 (2015).

[73] I. Al-Naib, J. E. Sipe, and M. M. Dignam, High harmonic generation in undoped graphene: Interplay of inter- and intraband dynamics, Phys. Rev. B **90,** 245423 (2014).

[74] X. Yao and A. Belyanin, Giant Optical Nonlinearity of Graphene in a Strong Magnetic Field, Phys. Rev. Lett. **108,** 255503 (2012).

[75] J. L. Cheng, N. Vermeulen, and J. E. Sipe, Third-order nonlinearity of graphene: Effects of phenomenological relaxation and finite temperature, Phys. Rev. B **91,** 235320 (2015).

[76] S. V. Morozov, K. S. Novoselov, M. I. Katsnelson, F. Schedin, D. C. Elias, J. A. Jaszczak, and A. K. Geim, Giant Intrinsic Carrier Mobilities in Graphene and its Bilayer, Phys. Rev. Lett. **100,** 016602 (2008).

[77] J.-H. Chen, C. Jang, S. Xiao, M. Ishigami, and M. S. Fuhrer, Intrinsic and extrinsic performance limits of graphene devices on SiO_2, Nat. Nanotechnol. **3,** 206 (2008).

[78] B. Rahmani, A. Bagheri, A. Khavasi, and K. Mehrany, Effective medium theory for graphene-covered metallic gratings, J. Opt. **18,** 105005 (2016).

[79] D. Pozar, *Microwave Engineering* (Wiley, New York, 1998).

[80] A. Bagheri, B. Rahmani, and A. Khavasi, Effect of graphene on the absorption and extraordinary transmission of light in 1-D metallic gratings, IEEE J. Quantum Electron. **53,** 1 (2017).

[81] W. L. Barnes, W. A. Murray, J. Dintinger, E. Devaux, and T. W. Ebbesen, Surface Plasmon Polaritons and Their Role in the Enhanced transmission of light through periodic arrays of subwavelength holes in a metal film, Phys. Rev. Lett. **92,** 107401 (2004).

[82] P.-Y. Chen, M. Farhat, and H. Bağcı, Graphene metascreen for designing compact infrared absorbers with enhanced bandwidth, Nanotechnology **26,** 164002 (2015).

[83] P.-Y. Chen and A. Alu, Terahertz metamaterial devices based on graphene nanostructures, IEEE Trans. Terahertz Sci. Technol. **3,** 748 (2013).

[84] See Supplemental Material at http://link.aps.org/supplemental/10.1103/PhysRevApplied.11.024050 for a detailed analysis of the effect of graphene electron relaxation time on the absorption and THG conversion efficiency, additional details about the numerical method used, the computed absorptance responses of planar gold substrates with and without graphene on top, and the demonstration of the computed power flow and resulting perfect absorption.

[85] J. B. Oostinga, H. B. Heersche, X. Liu, A. F. Morpurgo, and L. M. K. Vandersypen, Gate-induced insulating state in bilayer graphene devices, Nat. Mater. **7,** 151 (2008).

[86] K. S. Novoselov, A. K. Geim, S. V. Morozov, D. Jiang, Y. Zhang, S. V. Dubonos, I. V. Grigorieva, and A. A. Firsov, Electric field effect in atomically thin carbon films, Science **306,** 666 (2004).

[87] S. H. Lee, M. Choi, T.-T. Kim, S. Lee, M. Liu, X. Yin, H. K. Choi, S. S. Lee, C.-G. Choi, S.-Y. Choi, X. Zhang, and B. Min, Switching terahertz waves with gate-controlled active graphene metamaterials, Nat. Mater. **11,** 936 (2012).

[88] M. Walther, D. G. Cooke, C. Sherstan, M. Hajar, M. R. Freeman, and F. A. Hegmann, Terahertz conductivity of thin gold films at the metal-insulator percolation transition, Phys. Rev. B **76,** 125408 (2007).

[89] A. Ishikawa, T. Tanaka, and S. Kawata, Negative Magnetic Permeability in the Visible Light Region, Phys. Rev. Lett. **95,** 237401 (2005).

[90] E. Poutrina, C. Ciracì, D. J. Gauthier, and D. R. Smith, Enhancing four-wave-mixing processes by nanowire arrays coupled to a gold film, Opt. Express **20,** 11005 (2012).

[91] D. Chatzidimitriou, A. Pitilakis, and E. E. Kriezis, Rigorous calculation of nonlinear parameters in graphene-comprising waveguides, J. Appl. Phys. **118,** 023105 (2015).

[92] See Supporting Information in M. Parzefall and L. Novotny, Light at the end of the tunnel, *ACS Photonics* **5,** 4195 (2018).

[93] H. Nasari and M. S. Abrishamian, Nonlinear terahertz frequency conversion via graphene microribbon array, Nanotechnology **27,** 305202 (2016).

[94] B. Jin, T. Guo, and C. Argyropoulos, Enhanced third harmonic generation with graphene metasurfaces, J. Opt. **19,** 094005 (2017).

[95] P. U. Jepsen, R. H. Jacobsen, and S. R. Keiding, Generation and detection of terahertz pulses from biased semiconductor antennas, J. Opt. Soc. Am. B **13,** 2424 (1996).

[96] D. You, D. R. Dykaar, R. R. Jones, and P. H. Bucksbaum, Generation of high-power sub-single-cycle 500-fs electromagnetic pulses, Opt. Lett. **18,** 290 (1993).

[97] P. Genevet, J. P. Tetienne, E. Gatzogiannis, R. Blanchard, M. A. Kats, M. O. Scully, and F. Capasso, Large enhancement of nonlinear optical phenomena by plasmonic nanocavity gratings, Nano Lett. **10,** 4880 (2010).

[98] C. David, J. Bruder, T. Rohbeck, C. Grünzweig, C. Kottler, A. Diaz, O. Bunk, and F. Pfeiffer, Fabrication of diffraction gratings for hard X-ray phase contrast imaging, Microelectron. Eng. **84,** 1172 (2007).

[99] V. Rinnerbauer, S. Ndao, Y. Xiang Yeng, J. J. Senkevich, K. F. Jensen, J. D. Joannopoulos, M. Soljačić, I. Celanovic, and R. D. Geil, Large-area fabrication of high aspect ratio tantalum photonic crystals for high-temperature selective emitters, J. Vac. Sci. Technol. B **31,** 011802 (2013).

[100] L. J. Guo, Nanoimprint lithography: Methods and material requirements, Adv. Mater. **19,** 495 (2007).

[101] N. Rivera, I. Kaminer, B. Zhen, J. D. Joannopoulos, and M. Soljačić, Shrinking light to allow forbidden transitions on the atomic scale, Science **353,** 263 (2016).

[102] S. Sanders, A. May, A. Alabastri, and A. Manjavacas, Extraordinary enhancement of quadrupolar transitions using nanostructured graphene, ACS Photonics **5,** 3282 (2018).